EXPLOITING THE COHERENCE OF SEABED SCATTERING FOR REPEAT-PASS SAS MICRO-NAVIGATION

AJ Hunter University of Bath, Claverton Down Rd,
North East Somerset, BA2 7AY, United Kingdom;
a.j.hunter@bath.ac.uk
S Dugelay NATO STO, Centre for Maritime Research and Experimentation,
Viale San Bartolomeo 400, 19126 La Spezia, Italy;
samantha.dugelay@cmre.nato.int

1 INTRODUCTION

Synthetic aperture sonar (SAS) is an advanced technique for seabed inspection. It provides extremely high resolution images that are independent of range and frequency[1] and outperforms conventional sidescan sonar. However, the coherent data processing relies on sub-wavelength navigation precision to correctly focus the SAS images; uncompensated errors can result in severe degradation of image quality[2]. The redundant phase centre (RPC) micro-navigation algorithm is crucial for this.

The RPC algorithm operates on the echo data collected "through-the-sensor". It exploits the spatial coherence of the acoustic field scattered from the sediment to make precision estimates of the relative platform motion between subsequent pings[3]. These estimates provide the precision required for SAS processing – typically on order of mm or μm.

Repeat-pass interferometric imaging is a relatively new area of SAS research concerning the coherent processing of SAS data collected over repeated passes. It opens up several new capabilities, including coherent change detection for measuring very small (sub-wavelength) changes in the seabed[4] and the potential for higher resolution bathymetric mapping. However, it adds further challenges to the navigation problem since errors can accumulate significantly between passes.

In recent work, the RPC algorithm was generalised[5] to exploit the temporal (as well as spatial) coherence of the scattered field and this has permitted the precision estimation of the relative platform motion between pings from repeated passes. We term this new algorithm repeat-pass RPC micro-navigation. It has been demonstrated on repeat-pass SAS data collected by the MUSCLE[6] autonomous underwater vehicle (AUV) during the MANEX'14 sea trial of the NATO Center for Maritime Research and Experimentation (CMRE). Furthermore, the resulting estimates have been used to mutually focus and co-register images from repeated passes separated by periods of approximately 15 min.

In this paper, we investigate the constraints imposed on repeat-pass RPC micro-navigation by the limited spatial coherence of the sediment back-scattering. This provides some bounds for the tolerable geometrical differences of repeated passes. It also provides rough guidelines for operational use of the algorithm and / or control of the AUV.

2 REPEAT-PASS RPC MICRO-NAVIGATION

The conventional (single-pass) RPC algorithm operates by forming pairs of so-called *redundant phase centre arrays* from the phase centers of the sonar array that overlap in subsequent pings; this is illustrated in Fig. 1(a) for two separate passes. A cross-correlation between signals from an RPC array pair yields a correlation peak at a certain time delay. This time delay can be measured and related to the relative change in the platform's position and orientation between the pings.

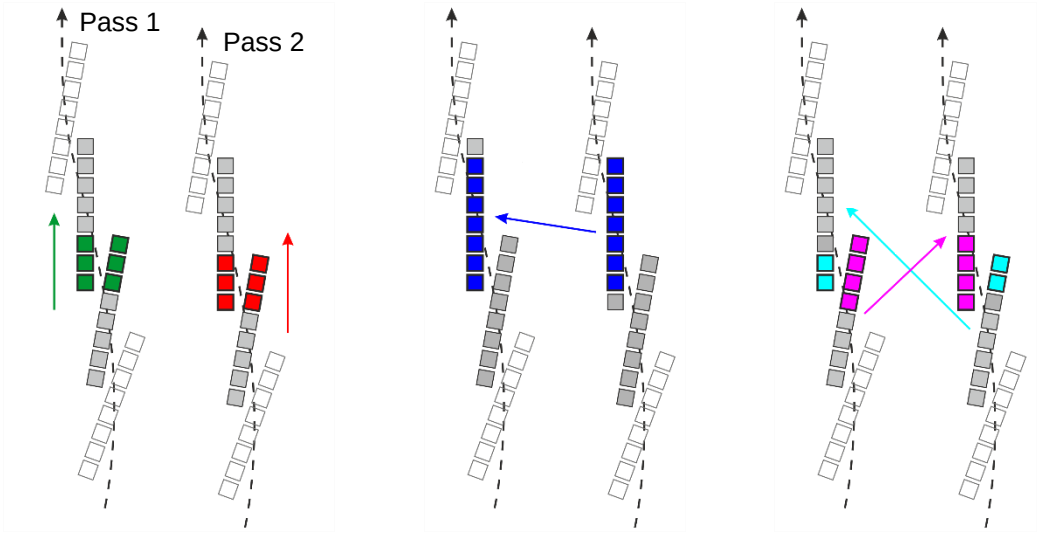

Figure 1 – *Geometry of (a) conventional RPC arrays formed for subsequent pings within the same pass (red and green) and (b,c) RPC arrays formed for corresponding pings between passes (blue, magenta, and cyan).*

Using this approach, it is possible to estimate surge and sway rates to sub-wavelength precision. Furthermore, the magnitudes of the peaks represent the signal coherence and provide a measure of the estimation quality. It is possible to also estimate yaw rate in this way, but it is typically less precise than measurements from the vehicle's inertial navigation system (INS). The trajectory of the vehicle is computed by accumulating the rate estimates (relative to a reference position and orientation) and this information is used to focus the SAS array.

Repeat-pass RPC micro-navigation is a generalisation that operates on RPC arrays formed between corresponding pings in separate passes as well as subsequent pings within the same pass. This is illustrated in Fig. 1 for two passes, where a total of five RPC array pairs (2 intra-pass and 3 inter-pass) can be formed for each ping. Cross-correlations between all five RPC array pairs for all P pings yields three over-determined systems of (5P-3) equations with 2P unknowns in surge, sway and yaw. These can be solved via weighted least-squares (using the signal coherence as weights) to yield the trajectories of the repeated passes in a common coordinate frame. Complete details of the algorithm are given Hunter *et al*. 2015[5].

A fundamental limitation of RPC micro-navigation is that it relies on the scattered acoustic field being sufficiently coherent so that a reliable peak can be observed when cross-correlating signals from RPC array pairs. This is particularly challenging for inter-pass pairs since: a) the relative geometry is not constrained by the momentum of the platform; and b) the time period between passes can be large resulting in temporal changes in the seabed.

3 THEORETICAL MODELS FOR COHERENCE LOSS

Each region of the seafloor presents a unique acoustic scattering pattern that is determined by its composition (i.e., distribution of scatterers) and the conditions under which it is insonified. The repeatability of the scattered signal can be quantified by the signal coherence

$$\gamma = \max\left\{ \left[\int_{-\infty}^{\infty} d_1^*(t) d_2(t+\tau)\,\mathrm{d}t \right] \Big/ \sqrt{\int_{-\infty}^{\infty} |d_1(t)|^2\,\mathrm{d}t \cdot \int_{-\infty}^{\infty} |d_2(t)|^2\,\mathrm{d}t} \right\}, \qquad (1)$$

where $d_1(t)$ and $d_2(t)$ are the signals from repeated measurements. The coherence will be unity under identical conditions and will decrease as the conditions change.

There are a number of potential contributors to coherence loss. These can be expressed as

$$\gamma = \gamma_F \times \gamma_B \times \gamma_N \times \gamma_T , \tag{2}$$

where the first two factors represent the geometrical effects of footprint mismatch and baseline decorrelation, the third factor represents decorrelation from noise and errors introduced during data acquisition and processing (e.g., ambient noise, beamforming phase errors, etc.), and the last factor is a temporal decorrelation due to changes in the environment.

To simplify the analysis, we can assume a static environment and neglect the temporal decorrelation. Clearly, this is invalid when the time difference is large between observations. Regardless, the temporal decorrelation has a complicated dependence on the seabed and water column properties and can vary heavily across locations; this has been treated elsewhere both experimentally[4] and theoretically[7]. To further simplify, we can assume a well-designed system with negligible noise and errors introduced during data acquisition and processing. Under these simplifying assumptions, the limitations on signal coherence are imposed by the geometrical effects caused by differences in the data collection geometry between passes, i.e.,

$$\gamma \approx \gamma_F \times \gamma_B . \tag{3}$$

3.1 RPC Array Footprints

Each instant of time in an echo signal corresponds to the scattering from a particular area (or, more generally, a volume) of seabed. This *footprint* is a geometric projection of the combined pulse shape and azimuth beampattern; this varies with the position and orientation of the sonar, the seafloor topography, and the elapsed time since transmission of the pulse.

Consider a pair of N overlapping phase centres from repeated passes with a relative sway Y and yaw Θ and expressed in a coordinate system local to the RPC array from the first pass. Also consider a planar seabed at a constant depth Z. This geometry is illustrated in Fig. 2. The range and azimuth angle from each array to each point $(x,y,-Z)$ on the seabed are given by

$$r_1 = \sqrt{x^2 + y^2 + Z^2} \quad , \tag{4}$$

$$\theta_1 = \tan^{-1}(x / y), \tag{5}$$

$$r_2 = \sqrt{x^2 + (y - Y)^2 + Z^2} \, , \tag{6}$$

$$\theta_2 = \tan^{-1}(x / (y - Y)) - \Theta . \tag{7}$$

The footprints of the RPC arrays from each pass can be represented as

$$a_n(x, y) = a_n^{(r)}(x, y) \cdot a_n^{(\theta)}(x, y), \tag{8}$$

where the subscript n denotes the first or second pass and the superscripts (r) and (θ) denote projections of the pulse shape and azimuth beampattern, respectively.

The projections of the pulse are given by

$$a_n^{(r)}(x, y) = \left| s\left((r_n - R_n) / c \right) \right| \tag{9}$$

where $s(t)$ is the transmitted signal and c is the speed of sound in water, R_1 is the range of interest

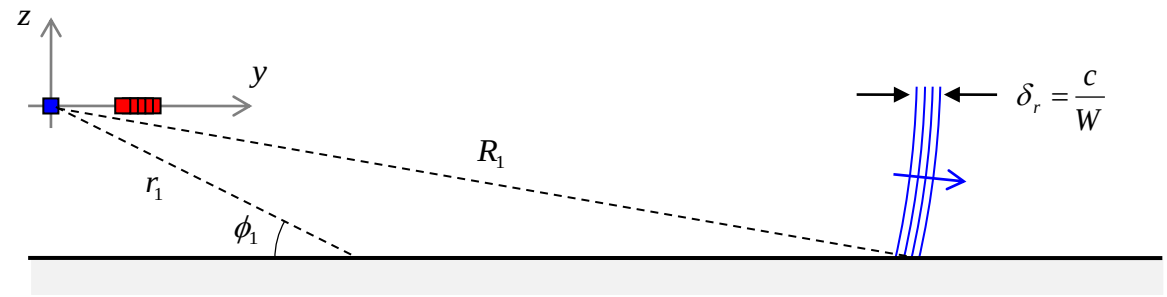

(a)

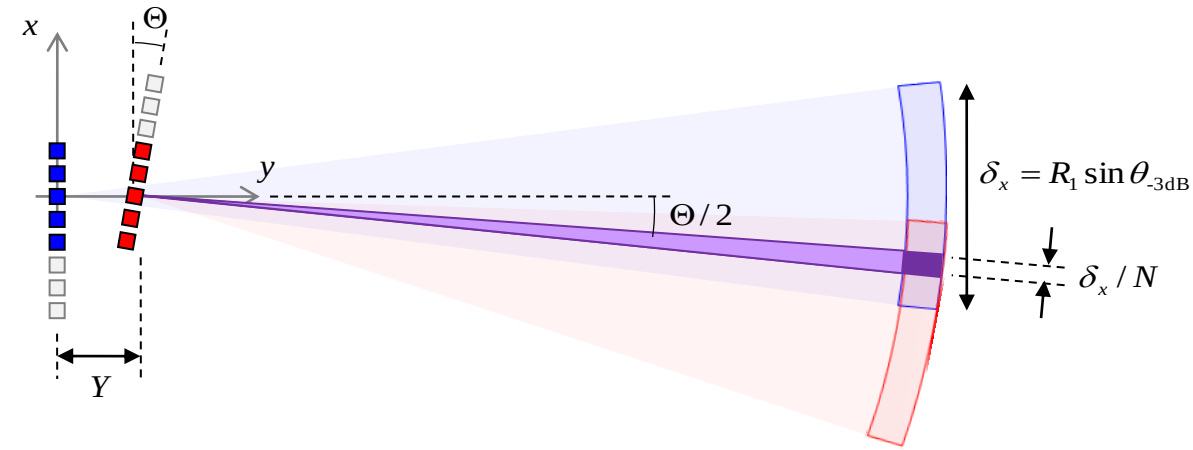

(b)

Figure 2 – *Geometry for an RPC array pair of N=5 overlapping phase centres with relative sway Y and yaw Θ. The phase centres, beams, and footprints of the individual transducers are represented in blue and red for the first and second pass; the common steered beam and footprint of both RPC arrays is in purple.*

relative to the first pass, and

$$R_2 = \sqrt{\left(\sqrt{R_1^2 - Z^2} - Y\cos(\Theta/2)\right)^2 + Z^2} \qquad (10)$$

is the corresponding range in the second pass. The temporal extent of the pulse $s(t)$ is inversely proportional to its bandwidth W.

The signal cross-correlation between the RPC array pair is maximised when both arrays are steered to the common azimuth angle bisecting the array normals. This yields azimuth projections of

$$a_1^{(\theta)}(x,y) = \left|B(\theta_1; -\Theta/2)\right|, \qquad (11)$$

$$a_2^{(\theta)}(x,y) = \left|B(\theta_2; \Theta/2)\right|, \qquad (12)$$

where $B(\theta;\alpha)$ is the beampattern for an N-element array with steering angle α. Note that the arrays can only be steered reliably within the limits imposed by the largest physical transducer, e.g., $|\alpha| < \theta_{\text{-3dB}}/2$ for a rectangular transducer of size D where $\theta_{\text{-3dB}} = \lambda/D$ is the -3 dB beamwidth and $\lambda = c/f$ is the wavelength at frequency f.

3.2 Footprint Mismatch

Signals from the RPC array pair correspond to a common point of interest on the seabed. However, in the presence of sway and yaw, the differences in projection conditions causes the projected shapes of the pulse and beampattern to differ. This results in a footprint mismatch. Any regions of the footprints that do not observe a common area of the seabed will, therefore, contribute to signal decorrelation.

The decorrelation due to footprint mismatch can be expressed as a ratio of the common area to the total area, i.e.,

$$\gamma_F = \left[\int_{-\infty}^{\infty} \int_{-\infty}^{\infty} a_1(x,y) a_2(x,y) \cdot \mathrm{d}x \cdot \mathrm{d}y \right] \Bigg/ \sqrt{\int_{-\infty}^{\infty} \int_{-\infty}^{\infty} a_1^2(x,y) \cdot \mathrm{d}x \cdot \mathrm{d}y \int_{-\infty}^{\infty} \int_{-\infty}^{\infty} a_2^2(x,y) \cdot \mathrm{d}x \cdot \mathrm{d}y} \ . \qquad (13)$$

3.3 Baseline Decorrelation

Although the arrays are steered towards a common point on the seabed (i.e., the centres of the footprints are co-located), the observation angles

$$\phi_1 = \sin^{-1}(Z / R_1), \qquad (14) \qquad\qquad \phi_2 = \sin^{-1}(Z / R_2) \qquad (15)$$

are different due to the relative sway (or baseline) between passes. The speckle pattern generated from the common footprint region is very sensitive to changes in observation angle. Therefore, this causes a decorrelation of the signal.

For a rough seabed modelled as a random distribution of scatterers, the decorrelation is given by the van Cittert-Zernike theorem[8]. This describes a Fourier relationship with the scattering area, i.e.,

$$\gamma_B = A\left(\frac{2}{\lambda} \sin(\phi_2 - \phi_1), \frac{2}{\lambda} \sin(\phi_2 - \phi_1) \right) \Big/ A(0,0) \qquad (16)$$

where

$$A(u,v) = \int_{-\infty}^{\infty} \int_{-\infty}^{\infty} a_1(x,y) a_2(x,y) \exp(-j2\pi(xu + yv)) \cdot \mathrm{d}x \cdot \mathrm{d}y \qquad (17)$$

is the 2-D Fourier transform of the common footprint.

4 RESULTS

During an experiment in the MANEX ’14 sea trial, the MUSCLE AUV made eleven repeated passes with a 1 deg heading increment and a time period of 16 min, 30 sec between each successive pass. The tracks of these passes are shown in Fig. 3(a). The resulting data provide a variety of inter-pass sway and yaw with values ranging from 0-25 m and 1-10 deg, respectively.

The repeat-pass RPC micro-navigation algorithm was applied to each of the 55 possible sets of repeated passes. Inter-pass correlations were only observed on the 19 sets separated by 1 deg or 2 deg heading increments. Fig. 3(b) and 3(c) show example intra-pass and inter-pass correlation results for pairs 1-2 and 1-3, which are separated by 1 deg and 2 deg, respectively. The inter-pass coherence is shown to attain a maximum value of approximately γ = 0.8 for pair 1-2, which is comparable to the average intra-pass value. The inter-pass coherence is reduced to a maximum of approximately γ = 0.6 for pair 1-3.

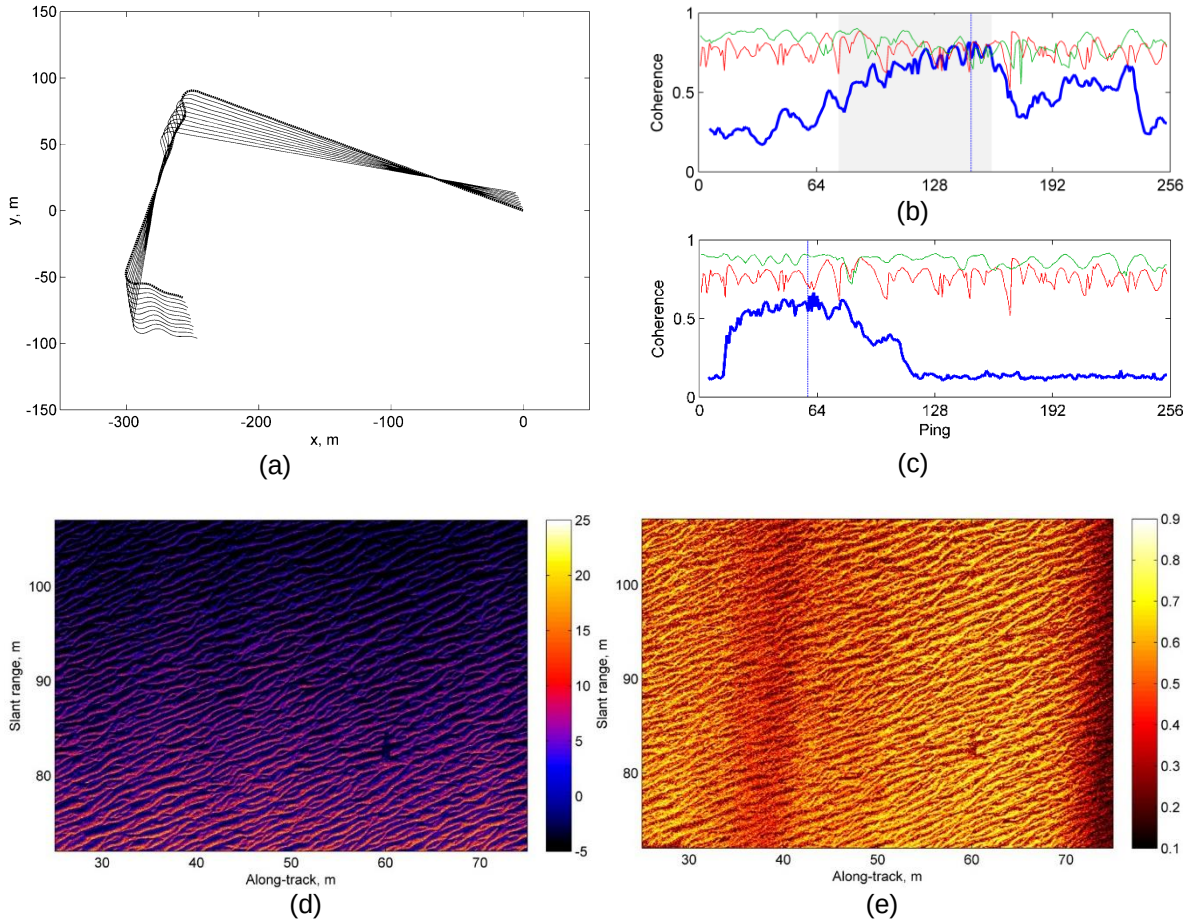

Figure 3 – *Experimental results from the MANEX '14 sea trial: (a) tracks of 11 repeated passes with 1 deg increments in heading (thick line is pass 1); intra-pass (red and blue) and inter-pass (blue) coherence for (b) passes 1 and 2 (1 deg increment) and (c) passes 1 and 3 (2 deg increment); (d) SAS image from pass 1 focused using repeat-pass RPC micro-navigation between passes 1 and 2; and (e) coherence map of the co-registered images.*

Fig. 3(d) shows an example SAS image from pass 1 that has been mutually focused with the image from pass 2 using repeat-pass RPC micro-navigation. Fig. 3(e) shows the coherence map between the co-registered images, demonstrating that a good overall registration is achieved. Some bands of low coherence are observed at 35-40 m and 70-75 m in along-track and we attribute these to large values of inter-pass sway or yaw at these track positions.

To understand the effects of sway and yaw on the inter-pass RPC coherence, we consider the values observed in the experimental results and compare these with the values predicted by the theory of Section 3.

The coherence and magnitudes of sway and yaw were computed for every inter-pass RPC array pair formed within the 19 sets. The population of all pairs with coherence greater than $\gamma = 0.2$ was arranged into sway and yaw bins of width 0.1 m and 0.2 deg, with a resulting distribution shown in the histogram of Fig. 4(a). The average of the coherence was then computed for all bins containing more than 10 samples, yielding the empirical relationship for the coherence versus sway and yaw shown in Fig. 4(e). The standard deviations of the coherence are also shown in Fig. 4(c). A clear trend can be observed with a maximum coherence of 0.8 at the lowest magnitudes of sway and yaw, decreasing towards zero beyond sway and yaw magnitudes of approximately 1.25 m and 3.5 deg.

The theoretical models of Section 3 were evaluated over the same sway and yaw bins using the parameters of the MUSCLE SAS[6] and the known geometry of the experiment. The MUSCLE SAS uses a centre frequency of 300 kHz and has a signal bandwidth of 60 kHz (giving a pulse length of δ_r=25 mm in the water after matched filtering). It has a transmit aperture of length 5 cm (imposing a -3 dB beamwidth of 5.8 deg) and a 36-element receiver array with apertures of length 3 cm (-3 dB beamwidth of 9.6 deg). RPC arrays with a variety of lengths can be formed on repeated passes depending on the particular alignment of the ping pairs. These can range from a worst case of N/2=18 overlapping phase centres to a best case of N=36; we assume the average of 3N/4=27. The altitude above the seabed was approximately 10 m.

The theoretical effect of decorrelation due to footprint mismatch is shown in Fig. 4(b), the effect of baseline decorrelation is shown in Fig. 4(d), and the total coherence is shown in Fig. 4(f). Comparison with the experimental results of Fig. 4(e) reveals a similar structure, but with higher values predicted compared to those measured in practice.

5. SUMMARY

The performance of the repeat-pass RPC micro-navigation algorithm depends on the level of inter-pass coherence. Experimental values of inter-pass coherence were measured for repeated passes of the MUSCLE SAS and these were compared with the theoretical values predicted by the geometrical effects of footprint mismatch and baseline decorrelation. We observed a reasonable agreement between experiment and theory and the discrepancies are thought to be caused by various factors that were ignored in the theoretical analysis, including: data acquisition and processing noise, temporal decorrelation of the environment, and relative altitude differences between the passes. This requires further investigation.

Based on the experimental results, sufficient inter-pass coherence can be achieved for the MUSCLE SAS when there is less than approximately 2 deg of yaw and 0.5 m of sway between passes. These limitations on the inter-pass geometry provide rough guidelines for the operational use of the algorithm.

ACKNOWLEDGMENT

This work was funded by the NATO Allied Command Transformation. The authors would like to thank the CMRE engineering department and the crew of the NRV Alliance for their support in collecting the experimental data during the MANEX ’14 trial. Dr. Hunter is grateful to CMRE for hosting him during the summer of 2014.

REFERENCES

1. M.P. Hayes and P.T. Gough, Synthetic aperture sonar: a review of current status, IEEE J. Ocean. Eng., 34(3), 207-224 (Jul 2009)
2. D.A. Cook and D.C. Brown, Analysis of phase error effects on stripmap SAS, IEEE J. Ocean. Eng., 34(3), 250-262 (Jul 2009)
3. R.W. Sheriff, Synthetic aperture beamforming with automatic phase compensation for high frequency sonars, In Proc. Symposium on Autonomous Underwater Vehicle Technology, Washington DC, USA (Jun 1992)
4. A. Lyons and D.C. Brown, The impact of the temporal variability of seafloor roughness on synthetic aperture sonar repeat-pass interferometry, IEEE J. Ocean Eng, 38(1), 91-97 (Jan 2013)
5. A.J. Hunter, S. Dugelay, and W.L.J. Fox, Repeat-pass SAS micro-navigation using redundant phase center arrays, IEEE J. Ocean. Eng., In Press. (2015).

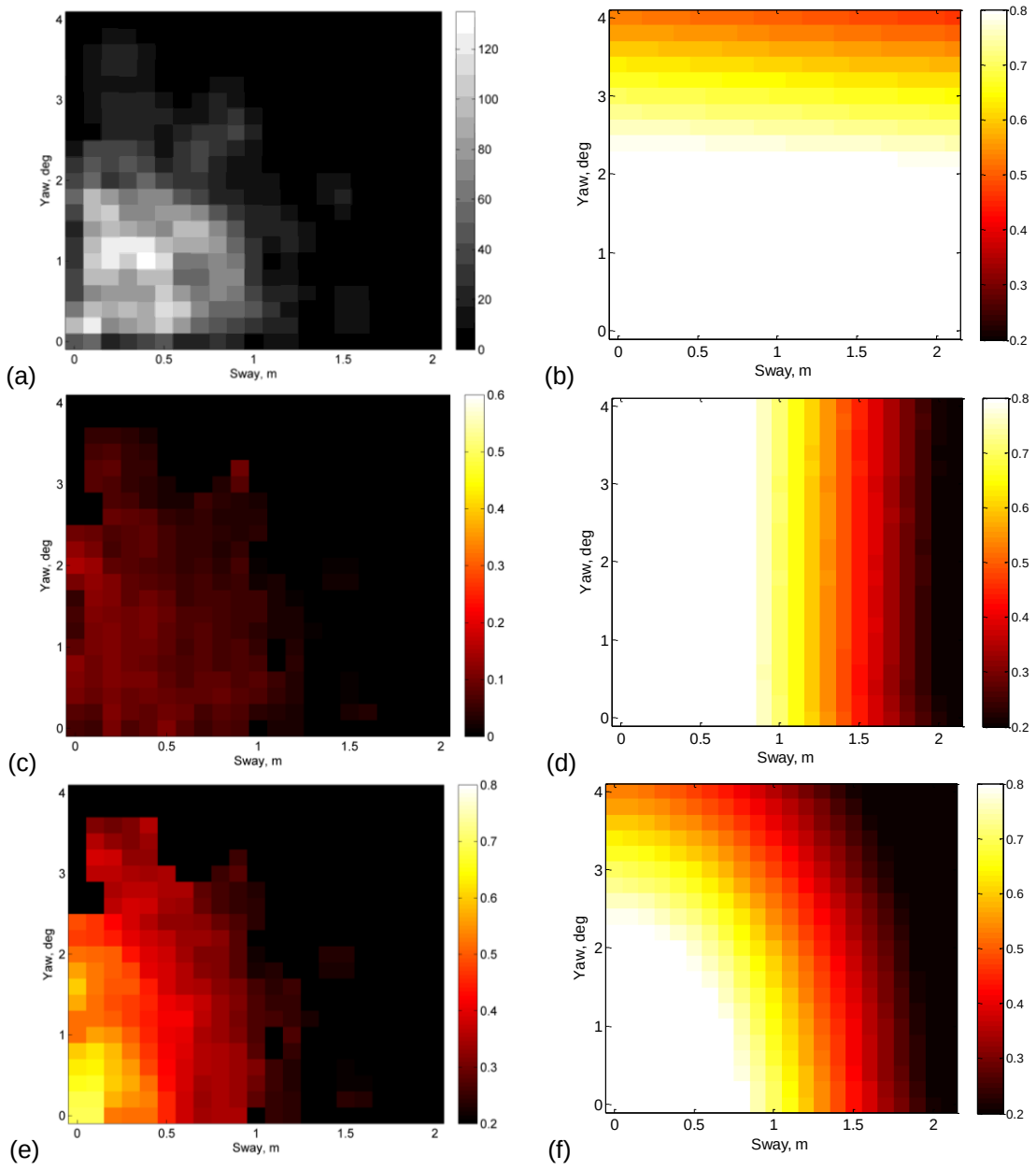

Figure 4 – Inter-pass coherence for the MUSCLE SAS as a function of relative sway and yaw. Experimental results: (a) histogram of ping pairs used to compute measurement statistics, (c) standard deviation of measurements, and (e) mean of measurements. Theoretical predictions for an RPC array of 27 elements: (b) effect of footprint mismatch, (d) effect of baseline decorrelation, and (f) total coherence.

6. M. Pinto, A. Bellettini, R. Hollett, and L. Wang, MUSCLE: A mine-hunting UUV with synthetic aperture sonar capability for littoral operations, In Proc. International Conference on Underwater Acoustic Measurements, Crete, Greece, (Jun 2005)
7. S.F. Johnson and A.P. Lyons, Simulation of rippled sand seafloor evolution for synthetic SAS imagery, In Proc. International Conference on Underwater Acoustic Measurements, Kos, Greece (2011)
8. R. Mallart and M. Fink, The van Cittert-Zernike theorem in pulse echo measurements, J. Acoust. Soc. Am., 90(5), 2718-2727 (Nov 1991)